PPPL-3311, Preprint: August 1998, UC-420, 423

Modeling of Tritium Retention in TFTR*

C.H. Skinner,[a] J.T. Hogan,[b] J.N. Brooks,[c] W. Blanchard,[a] R.V. Budny,[a] J. Hosea,[a] D. Mueller,[a] A. Nagy,[a] and D.P. Stotler[a]

[a]*Princeton University, Plasma Physics Laboratory, Princeton NJ 08543*
[b]*Oak Ridge National Laboratory, Oak Ridge, TN 37831.*
[c]*Argonne National Laboratory, Argonne, IL 60439.*

Abstract:

The Tokamak Fusion Test Reactor tritium retention experience is reviewed and the data related to models of plasma surface interactions. Over 3.5 years of TFTR DT operations, approximately 51% of the tritium injected into TFTR was retained in the torus. Most of this was subsequently recovered by glow discharges and air ventilation. Co-deposition rates for representative conditions in tritium operation were modeled with the BBQ code. The calculations indicate that known erosion mechanisms and subsequent co-deposition are sufficient to account for the order of magnitude of retention.

1. Introduction

Tritium retention is recognized to be a critical issue in DT burning fusion devices, particularly those with graphite first walls. Two major tokamaks, the Tokamak Test Fusion Reactor (TFTR) and the Joint European Torus (JET), have now operated with tritium fuel and experienced relatively high levels of tritium retention. Over 3.5 years of TFTR DT operations, approximately 51% of the tritium supplied to the plasma was retained in the vacuum vessel [[1]-[234]]. Most of this was later removed in cleanup campaigns. In JET, 20%-40% of the tritium supplied in the recent DTE1 experiments was retained during plasma operations[[5]]. Data on the retention of tritium produced in DD reactions is also available from machines operating with deuterium. In JT-60, the tritium retention was 70%-80%, as measured from the tokamak exhaust[[6]], while in DIII-D, a retention fraction of 10-20% was found in the vessel tiles[[7]]. The tritium experience in large tokamaks and its application to ITER was the subject of a recent workshop[[8]]. The tritium fueling requirements of ITER are much higher than present tokamaks because of its larger size and much longer pulse duration, however modeling predicts a much lower retention fraction for ITER[[9]]. The fraction of tritium retained in ITER must be much lower than that experienced in present tokamaks and techniques for rapid tritium removal need to be developed for ITER maintain a reasonable

operational schedule. For a future DT fusion reactor to be self-sufficient in tritium the fraction of tritium permanently retained will have to be less than 0.1%[10]. Comparison of the TFTR experience to modeling can provide tests that will narrow the uncertainties and help deepen the understanding of tritium retention in the complex environment of the plasma edge.

Tritium retention is a result of atomic and molecular processes occurring as the edge plasma interacts with the surface of plasma facing components. While some aspects of the individual processes such as sputtering can be studied in laboratory experiments, the characteristics of surface and the edge plasma in a tokamak are determined by their mutual interaction in a complex non-linear environment that is difficult to diagnose and to model. Projections of tritium retention are typically derived from prior experience with deuterium[11,12]. To date, there have not been first principles models of retention that have predicted the observed levels of retention in tokamaks. In TFTR, the relatively sparse edge diagnostics and complex discharge history pose additional challenges. However, because of the importance of the retention issue, and the extensive experience of TFTR in operating with tritium, closer examination of basic processes governing TFTR tritium retention seems warranted. Thus, this paper aims to link the available TFTR retention database to models similar to those used in ITER predictive modeling to better understand similarities in tritium retention processes, as well as differences between TFTR conditions and operation under detached divertor conditions.

2. TFTR tritium experience

TFTR had 3.5 years of experience with tritium fueling and removal. Over this period, 100 g of tritium was processed and 5 g of tritium supplied to the plasma by neutral beam injection and direct gas puffs. The tritium fueling history is shown in Table 1 and is documented in detail in Refs. [1-4]. Overall, during the three periods of DT plasma operations (excluding periods of active tritium removal), approximately 51% of the tritium fuel was retained in the torus. Active tritium removal by glow discharge and air ventilation was successful in removing substantial amounts of tritium in between periods of plasma operations.

In preparation for DT operation, extensive measurements were made of in-vessel components exposed to deuterium to provide guidelines for the DT campaign. Analysis of in-vessel components during the deuterium phase showed the main mechanism for retention was co-deposition of deuterium with carbon[13,14]. Since the global tritium retention during the DT campaign was similar to the deuterium retention measured earlier, we assume that the distribution of tritium in the vessel is similar to that measured for deuterium. Eleven bumper limiter tiles exposed to TFTR DT operations have been recently removed for analysis; however, at the present time, the results are not yet available.

3. Co-deposition rates for deuterium operation (previous modeling studies with the REDEP code)

Analyses of sputtering erosion/redeposition were performed for various TFTR carbon bumper limiter configurations, and ohmic and beam heating shots using the REDEP code [15]. This code computes the transport of sputtered impurities in the near-surface plasma region using a finite difference method with iteration to solve a system of coupled integral equations relating hydrogen isotope ion sputtering, redeposition, and self-sputtering for points on the limiter surface. A trace-impurity, kinetic approach, with gyro-orbit averaging is used. Since plasma scrapeoff layer data was not available the required plasma parameter input to the code (density, temperature, etc. profiles) were inferred from plasma data at the closest boundary point. A three-dimensional REDEP analysis of the limiter, using then-typical beam heating shots (limiter boundary parameters: $n_e(a) = 5x10^{19}$ m^{-3}, $T_e(a) = 0.2$ keV, deuterium fuel) showed a spatially complex erosion profile, with peak erosion and peak growth rates of about 2 nm/s [16]. Subsequent work with "supershot" parameters (generally lower density, higher edge temperature) showed peak growth rates approaching ~1 nm/s but with very high sensitivity to the plasma scenario for this regime.

4. Codeposition rates for tritium operation (modeling studies with the BBQ code)

In order to relate the role of co-deposition (and concomitant tritium retention) to the growth of co-deposited layers, it is necessary first to estimate the rate of erosion of carbon from the main TFTR plasma-facing component, the inner bumper limiter. This has been done by modeling selected characteristic TFTR discharges to estimate the carbon generation rates in these conditions. These data are then compared to the observed tritium retention. The carbon erosion/redeposition rate required to codeposit the amount of tritium retained is estimated and compared to BBQ predictions.

4.1 BBQ impurity generation model

BBQ is a 3D Monte Carlo code which characterizes the evolution of carbon impurities generated by plasma surface interactions [17]. The particle dynamics model in BBQ is patterned after the LIM [18] and REDEP codes[15]. Rates for impurity generation due to physical sputtering of C by D^+ and C^{n+}, are taken from [19], for chemical sputtering from [20] and for radiation-enhanced sublimation (RES) [21]. For the generation of methane (or methyl radicals) through chemical sputtering, the Erhardt-Langer ionization and dissociation rates for the CH_n^{m+}through C^{n+} break-up chain [22] are used. The dependence of these processes on incident D^+ particle flux is assumed to be that of Roth et al. [19].

Two effects are present for TFTR limiter conditions which are not encountered in modeling detached divertors: sensitivity to the detailed geometry of the inner bumper tile configuration and a

sensitive dependence on scrape-off layer diffusivity. The latter is a feature of the 'attached' condition of these limiter plasmas, and differs from detached divertor plasmas, for which thermal conduction (by definition) plays a marginal role. To treat the first effect, the code uses detailed measurements of in-vessel components compiled in a computer aided design (CAD) file[23]. Using the exact geometry is important for large-area limiters since the near alignment of flux surfaces with the inner bumper limiter results in particle and heat fluxes which depend critically on the small angle of incidence of field lines with respect to this edge structure. For the same reason, detailed information regarding the noncircularity of strongly beam-heated plasmas is also needed. Ellipticities (or oblateness) (κ) of a only few % can modify the local fluxes by factors 2-5. For the second cited effect, consideration of non-zero perpendicular diffusivity in the scrape-off layer (which arises either through turbulent transport, or momentum-nonconserving charge exchange collisions) leads to an effective dependence of the incident particle flux density on the radial transport rate in the scrape-off layer (SOL). In general, the incident ion flux is given by $\Gamma = \Gamma_{ll}(0) \sin\theta \exp(-\rho/\lambda_\Gamma) + \Gamma_\perp(0) \cos\theta \exp(-\rho/\lambda_\Gamma)$, where $\theta = 0^\circ$ when the flux surface is tangential to the limiting surface, ρ is the minor radius measured from the last closed flux surface (LCFS), λ_Γ is the SOL decay length of the incident particle flux density and $\Gamma_{\perp,ll}(0)$ are the perpendicular and parallel (to **B**) particle flux densities at the LCFS. Thus, the incident particle flux is $\Gamma = \Gamma_{ll}(0)\, e^{-\rho/\lambda\Gamma} \sin(\theta+\alpha)$, with $\alpha \equiv \tan^{-1}[\Gamma_\perp(0) / \Gamma_{ll}(0)]$ so that α can be interpreted as the effective 'minimum angle of incidence'. We obtain magnetic configuration information from TRANSP [24] simulations of typical conditions, using a moments equilibrium description to determine the ellipticity of the last closed flux surface. For the effective angle of incidence we vary $\Gamma_\perp(0) / \Gamma_{ll}(0)$ from 0.4 to 0.001. The first value, 0.4 is a result obtained by consideration of a similar inner bumper limiter configuration in Tore Supra [25] and 0.001 is a value which has been found to model D_α distributions on the TFTR inner wall, as described below.

Table 2 shows the parameters from the representative discharges used for detailed modeling. Of these 76528 and 76530 are typical 'supershots', with DT and D-only neutral beam injection (NBI) respectively. These discharges are fueled predominately by NBI and recycling, there is no gas feed after the initiation of the discharge. Over the DT period there were many more deuterium neutral beam fueled discharges than tritium fueled discharges, the fueling ratio was T / (T + D) = 2 %. The isotopic composition of the plasma edge with DT neutral beam injection was mostly deuterium as evidenced by spectroscopic measurements of the isotopic fraction of tritium in Balmer-alpha emission [26]. The $T_\alpha/(H_\alpha+D_\alpha+T_\alpha)$ ratio as measured at the midplane for 76528 was 1% (+2%-1%). This is broadly consistent with the TRANSP modeling where the isotopic density ratio was 5% T in the outermost zone at the last closed flux surface. The third case is the ohmic target plasma before neutral beam injection in 76530. The fourth case is a supershot with relatively unconditioned walls. The fifth case is from an L-mode campaign in which large quantities of tritium were puffed directly into the plasma.

The values of λ in Table 2 were derived by a comparison of measurements of the poloidal distribution of H-alpha with modeling. The Balmer-alpha intensity is measured by 5 telescopes ("HAIFA system") viewing 3 cm diameter areas at different poloidal locations on the inner limiter and wall[27]. The DEGAS Monte Carlo neutral transport code [28] was used to model representative plasmas listed in Table 2. In DEGAS, hydrogenic neutrals are generated by dissociation, sputtering, reflection or charge-exchange. The plasma and mesh for TFTR simulations are taken from runs of the TRANSP interpretive code. The scrape-off layer is not modeled by TRANSP but is described using a radial scale length, λ, and a perpendicular diffusion parameter, δ. Their values are derived by comparing the simulated and measured poloidal D_α emission distribution [29].

4.2 BBQ results

The operational range of the TFTR tritium campaigns is quite wide and a large range of conditions was encountered. In spite of the great range of possible sources of carbon which could lead to co-deposition sinks, the mechanisms can be reduced to a smaller number by consideration of the basic features of physical sputtering, chemical sputtering and radiation-enhanced sublimation (RES). Fig. 1 shows some characteristics of the TFTR inner bumper limiter which must be taken into account when comparing TFTR tritium retention through co-deposition with results in divertor configurations or predictions for ITER. Fig 1(a) shows a typical magnetic flux surface geometry and the details of tile structure at one toroidal location. Fig. 1(b) shows the variation in the angle of field line incidence for the upper half of the limiter: the 'sawtooth' pattern is caused by the fact that the inner limiter is constructed from flat plate segments. Another notable feature is the presence of leading edges at poloidal angles +/- 60°. These areas are distant from the last closed flux surface, but can receive a significant flux for large plasmas and conditions in which the SOL decay length is large. Fig. 1(c,d) compares the poloidal distribution of incident heat flux to the limiter for values of $[\Gamma_\perp (0) / \Gamma_{ll}(0)] = 0.4$ and 0.001, respectively. The dashed line, for comparison, is the result for an assumed perfectly smooth inner bumper. The incident heat flux distribution has a flat profiles in poloidal angle for the case $[\Gamma_\perp (0) / \Gamma_{ll}(0)] = 0.4$, while the local heat flux at the upper (and lower, not shown) leading edge is increased by an order of magnitude for the case $[\Gamma_\perp (0) / \Gamma_{ll}(0)] = 0.001$. Fig 1 (c,d) also shows a calculation from BBQ of the simulated signal which would be seen by the HAIFA spectroscopic system for these two cases. The measured poloidal dependence is not very sensitive to $\Gamma_\perp (0) / \Gamma_{ll}(0)$. However, wide area infra-red views have seen evidence of strong local recycling at the upper and lower leading edges.

Figures 2 and 3 compare the impurity source distributions for the cases described in Table 2, for values of $[\Gamma_\perp (0) / \Gamma_{ll}(0)]=0.4$ and 0.001, respectively. As can be seen, the impurity source distributions, which are normalized to the incident D^+ flux, have generally similar and generally flat profiles in poloidal angle for the case $[\Gamma_\perp (0) / \Gamma_{ll}(0)]=0.4$. For the case $[\Gamma_\perp (0) / \Gamma_{ll}(0)]=0.001$, there is increased localization near the upper and lower leading edges of the inner bumper limiter.

BBQ redeposition calculations with these emission profiles indicate that ~60% of the sputtered impurities are promptly redeposited near the emission locus. This redeposition fraction is higher for RES and chemical sputtering since chemically and RES-produced impurities are emitted at wall thermal energies, and have a smaller range than the more energetic physically-sputtered impurities. Thus, redeposition of carbon can be expected to be peaked in these regions. The magnitudes of mean erosion yields are in the range of 0.02-0.04, which represents an effective physical sputtering yield in line with typical laboratory values[30]. The values at the higher end of this range represent impurity emission from the leading edge at high poloidal angles ($\theta = \pm 60°$).

Previous measurements of deuterium retention in TFTR found retention in the gaps between tiles and on the vessel wall. For example, it was found that retention in gaps was about 1/3 that on plasma facing surface even though the area of gaps was ≈30 times less. However, in the period 1992-1993 TFTR conducted an extensive re-alignment campaign for the inner bumper limiter, and the leading edge exposure between tiles was greatly reduced [23]. Thus, for the first approximation, gap deposition has not been included in the present estimates of tritium retention due to codeposition and is the subject of ongoing work.

5. Comparison of tritium retention predicted by modeling to that observed in TFTR.

The tritium retention fraction was observed to vary depending on whether the plasma was fueled by tritium neutral beams or tritium puffs. We focus on the effect of neutral beam injection by considering the period from November 1993 to August 1995, when nearly all of the tritium (3.8×10^{23} tritons) was injected into the torus via the neutral beams (including 6% cold gas) and only a trace amount (4.2×10^{21}) was injected by gas puff. By comparing the tritium injected with that recovered, the tritium inventory in the torus was estimated to be 1.3×10^{23} tritons. According to earlier tile measurements 44% of the deuterium retained in the torus was in a codeposited layer on plasma facing tile surfaces. If we assume that the tritium spatial distribution was similar to that with deuterium then 5.8×10^{22} tritons are expected to be in co-deposited layers on the plasma facing tile surface.

To relate the measured tritium retention to the BBQ modeling results we note that in TFTR the CII emission increases with neutral beam power, as did the deuterium retention[3]. We make the approximation that the tritium codeposition is linearly related to the neutral beam tritium fluence. Tritium neutral beam injection summed over the period November 1993- August 1995 was 1,826 source-seconds. There are 4 neutral beam boxes on TFTR each with 3 ion sources and nine sources were used for discharge #76528 of Table 2. We derive a tritium codeposition rate for a nine source tritium NBI discharge of 2.9×10^{20} tritons/s. Previous tile measurements showed a

with a D/C atomic ratio of approximately 0.2[13]. We assume that this fraction is maintained with tritium and hence the carbon deposition rate needed to retain the tritium is 1.4 x10^{21} C atoms/s.

In the BBQ modeling information on the D flux crossing the last closed flux surface is input from TRANSP. The D flux incident on the tile surfaces is amplified by a flux amplification factor, F, and previous DEGAS / B2 studies [31] have indicated values in the range F = 1-5. The value of F needed for the BBQ D flux to match that needed to trap the measured tritium retained is F = 3 - 8. The similarity between the amplification factor needed to bring BBQ into agreement with the measured retention and that expected in limiter machines is gratifying but must be treated with caution considering the approximations used in the analysis.

Figure 4 compares the poloidal variation of impurity sources from physical sputtering, chemical sputtering and RES, each using the same incident plasma and varying the wall temperature to give the maximum emission for each mechanism. As can be seen, the RES and chemical sputtering sources are localized closest to the equator since this is the region of greatest heat input and highest wall temperature. The effective sputtering yields for chemical erosion at the temperature and location of maximum yield can be five to ten times higher than the physical sputtering yields used in the previous estimate (Figs. 2 and 3), and those for RES can exceed the physical sputtering yields by factors up to 100. The chemical sputtering and RES sources thus have the potential magnitude to contribute significantly to retention during off normal conditions at elevated temperatures.

6. Comparison and implications for ITER

There are of course a number of significant differences between TFTR and ITER. While the power flux is not too different, (3 MW/m^2 for ITER compared to 1-3 MW/m^2 for TFTR) the peak erosion rate simulated for ITER is 0.5 m/burn year [9] or 16 nm/s, several times higher than the rate in TFTR. This is due to the characteristics of detached operation: rather high density and low temperature. In TFTR chemical erosion leads to high local redeposition; this material in turn, can be re-sputtered and eventually migrate to cooler regions, particularly at high poloidal angle, where, because of reduced incident D^+ flux, it can remain. In contrast, at the location of peak erosion in ITER simulations, on the order of 10% of the chemically sputtered carbon is lost, due to non-ionization of the end-of-hydrocarbon-chain carbon neutrals. The ITER design has a divertor, unlike TFTR, so that larger flux amplification can be obtained (divertor tokamaks, such as DIII-D, have considerable local flux amplification (~ 10-30) at the divertor plate).The largest difference between ITER and TFTR is in the pulse duration. ITER's pulse duration of 1,000 s is orders of magnitude larger than current tokamaks, and this increase is a much larger difference than the change in other core plasma parameters such as confinement time. This long pulse duration leads to

erosion rates of the order of cm per operation-year compared to tens of microns in present tokamaks and this in turn leads to the retention of large amounts of tritium in co-deposited layers.

7. Conclusions

Understanding and controlling tritium retention is essential to the operation of long pulse DT tokamaks. We have made some preliminary comparisons of modeling to the retention experienced in TFTR. The calculations suggest that known erosion mechanisms are sufficient to account for the order of magnitude of retention due to codeposition. Significant contributions from resputtered material, originally eroded by RES or chemical sputtering, are expected. The calculations suggest that when detailed analysis of TFTR tiles from the tritium campaign is made, that significant concentrations of co-deposited tritium will be found near the upper and lower leading edges of the bumper limiter.

The present comparison is hampered by the lack of detailed diagnostics of the edge plasma conditions and lack of shot by shot measurements of retention. However, although imperfect, comparisons of available measurements of retention in tokamaks with detailed models are an essential step to benchmark the codes and raise confidence in their predictions for future machines. To make further progress in this critical area, real-time in-vessel diagnostics need to be further developed and more widely implemented with dedicated run time. The detailed data generated will challenge models, lead to a better understanding of the many interacting plasma, atomic and surface phenomena involved and generate more confident predictions of retention in future devices.

Acknowledgments:

We would like to acknowledge fruitful discussions with G. Federici and M. Sugihara of the ITER JCT. This work was supported by the US DOE Contract Nos. DE-AC02-76CH03073 and W-31-109-ENG-38.

Table 1. Tritium fueling and removal history of TFTR.

Period	Number of tritium fueled discharges (NB+puff).	Tritium fueling by neutral beam injection (g)	Tritium fueling by gas puff (g)	Tritium removal from torus (g)	Tritium removal from neutral beam boxes (g)	TFTR inventory (g)
11/93 - 8/95	530	1.9	0.02			0.71
9/95	178	0.24	1.12			1.71
10/95 - 1/96				- 0.91	- 0.05	0.75
1/96 - 8/96	190	0.57	0.27			1.56
9/96 - 11/96				- 0.39	- 0.10	1.07
12/96 - 4/97	223	0.36	0.71			1.83
4/97 - 4/98				-0.50	-0.48	0.85

Table 2. Parameters for representative discharges used for detailed modeling. λ is the scale length for the exponential fall off in density and temperature outside the LCFS. Values of n_e, T_e, n_i, T_{imp} are from TRANSP for ρ/a =0.975. '76528a07' denotes the 7th TRANSP run for shot 76528.

Condition	Shot/ TRANSP run	Time s	λ (cm)	κ	n_e (cm^{-3})	T_e (keV)	n_i (cm^{-3})	T_{imp} (keV)
DT supershot 22 MW NBI	76528a07	3.45	1.3	1.031	$9.9\ 10^{12}$	0.66	$7.4\ 10^{12}$	1.89
D supershot 22 MW NBI	76530a22	3.45	1.3	1.023	$9.3\ 10^{12}$	0.59	$7.1\ 10^{12}$	1.81
ohmic target	76530a57	2.5	0.75	1.056	$3.7\ 10^{12}$	0.20	$1.9\ 10^{12}$	0.58
unconditioned D supershot 19 MW NBI	76649a04	4.2	1.6	1.046	$8.4\ 10^{12}$	0.44	$6.5\ 10^{12}$	1.24
L-mode w/T puff	88615a14	3.9	1.3	1.046	$1.2\ 10^{13}$	0.42	$1.1\ 10^{13}$	0.58

Figure Captions:

Figure 1 Characteristics of the TFTR bumper limiter. (a) Inner bumper geometry, showing discrete tile location and flux surfaces; (b) field line angle of incidence as a function of poloidal angle for the upper half; (c, d) heat flux deposition profiles vs poloidal angle for the upper half, for cases $\Gamma_{\perp}(0) / \Gamma_{ll}(0) = 0.4, 0.001$; the simulated $D\alpha$ signal from HAIFA spectroscopy for flux distributions are shown as dashed lines

Figure 2 Calculated local effective sputtering yield distributions (emitted impurity flux / incident D^+ flux) for the four cases of Table 2, with $\Gamma_{\perp}(0) / \Gamma_{ll}(0) = 0.4$

Figure 3 Calculated local effective sputtering yield distributions (emitted impurity flux / incident D^+ flux)for the four cases of Table 2, with $\Gamma_{\perp}(0) / \Gamma_{ll}(0) = 0.001$

Figure 4 Calculated local effective sputtering yield distributions (emitted impurity flux / incident D^+ flux, %) for (top) physical sputtering, (middle) chemical sputtering ($T_{wall}^{max} = 1000$ K) and (bottom) radiation-enhanced sublimation (RES) ($T_{wall}^{max} = 1600$ K)

References

[1] C.H. Skinner et al., J. Vac. Sci. Technol. **A14** (1996) 3267-3274.

[2] C.H. Skinner et al., J. Nucl. Mater. **241-243** (1997) 214-226.

[3] D. Mueller, et al., in 17th IEEE/NPSS Symposium on Fusion Engineering, IEEE, Piscataway, NJ, USA (1998) (Proc. 17th IEEE/NPSS Symposium, San Diego, Oct. 6-10, 1997), vol.1 p.279.

[4] A.Nagy et al, in 17th IEEE/NPSS Symposium on Fusion Engineering, IEEE, Piscataway, NJ, USA (1998) (Proc. 17th IEEE/NPSS Symposium, San Diego, Oct. 6-10, 1997), vol.1 p.317.

[5] P. Andrew et al., this conference.

[6] N. Miya, M. Nemoto, and N. Toyoshima, Fusion Technology **26** (1994) 507.

[7] P.L. Taylor, A.G. Kellman, and R.L. Lee, J. Fusion Energy **12** (1993) 35.

[8] C.H. Skinner, C. Gentile, J. Hosea et al., "Tritium Experience in Large Tokamaks: Application to ITER" Nucl. Fusion, to be published.

[9] J. N. Brooks et al. this conference.

[10] M.A. Abdou, E.L. Vold, C.Y. Gung et al., Fusion Technology, 9 (1986) 250

[11] A.E. Pontau, D.K. Brice, D. A. Buchenauer, Fus. Eng. and Design **10** (1989) 365-371.

[12] A. Rossi et al. this conference.

[13] W.R.Wampler, B.L.Doyle, S.R.Lee et al., J. Vac. Sci. Technol. **A6** (1988) 2111; H.F.Dylla, K.L.Wilson, Princeton Plasma Physics Laboratory Report, PPPL-2523, April 1988.

[14] R.A. Causey, J. Nucl. Mater. **162-164** (1989) 151-161.

[15] R.T. McGrath, J.N. Brooks, J. Nucl. Mater. **162-164** (1989) 330.

[16] T.Q. Hua, J.N. Brooks, J. Nucl. Mater. **196-198** (1992) 514. Note: corrected units for Figs. 5 and 7 are 100 Å/s (T.Q. Hua, Argonne National Laboratory, personal communication

1998).

[17] J. Hogan, C.C. Klepper, J. Harris et al., Proceedings of the 16th International Conference on Fusion Energy, Montreal, 7-11th October 1996, V.2, 625 IAEA, Vienna, 1997.

[18] P. Stangeby, Contrib Plasma Phys. **28** (1998) 507.

[19] J. Roth and C. Garcia-Rosales, Nucl. Fusion **36** (1996) 1647.

[20] B.V. Mech, A.A. Haasz, J.W. Davis, J. Nucl. Mater**. 241** (1997) 1147.

[21] J. Roth, E. Vietzke, A.A. Haasz, Suppl. Nucl. Fusion, **1** (1991) 63.

[22] A.B. Ehrhardt , W.D. Langer "Collisional Processes of Hydrocarbons in Hydrogen Plasmas," Princeton Plasma Physics Laboratory Report PPPL-2477, 1987.

[23] M.D. McSmith, G.D. Loesser, D.K. Owens, Fus. Technol. **26** (1994) 498.

[24] R.V. Budny, Nucl. Fusion **34** (1994) 1247.

[25] D. Guilhem et al., Proceedings of the 15th International Conference on Fusion Energy, Sevilla, October 1994, V.1, 839 IAEA, Vienna, 1995.

[26] C.H. Skinner et al., Nucl. Fusion **35** (1995) 143-151.

[27] A.T. Ramsey and S.L. Turner, Rev. Sci. Instrum. **58** (1987) 1211.

[28] D.P. Stotler, C.H. Skinner, R.V. Budny, A.T. Ramsey, D.N. Ruzic, R.B. Turkot, Phys. Plasmas **3** (1996) 4084.

[29] C.H. Skinner, M.G. Bell, R.V. Budny, D.L. Jassby, H. Park, A.T. Ramsey, D.P. Stotler, and J.D. Strachan, Phys. Plasmas **5** (1998) 1062-1067.

[30] W. Eckstein, Max Planck Institute für Plasmaphysik, Report IPP/209, March 1998

[31] D. Stotler et al., Proc. IEEE Meeting on Plasma Science (Oakland), (1989) p. 88.

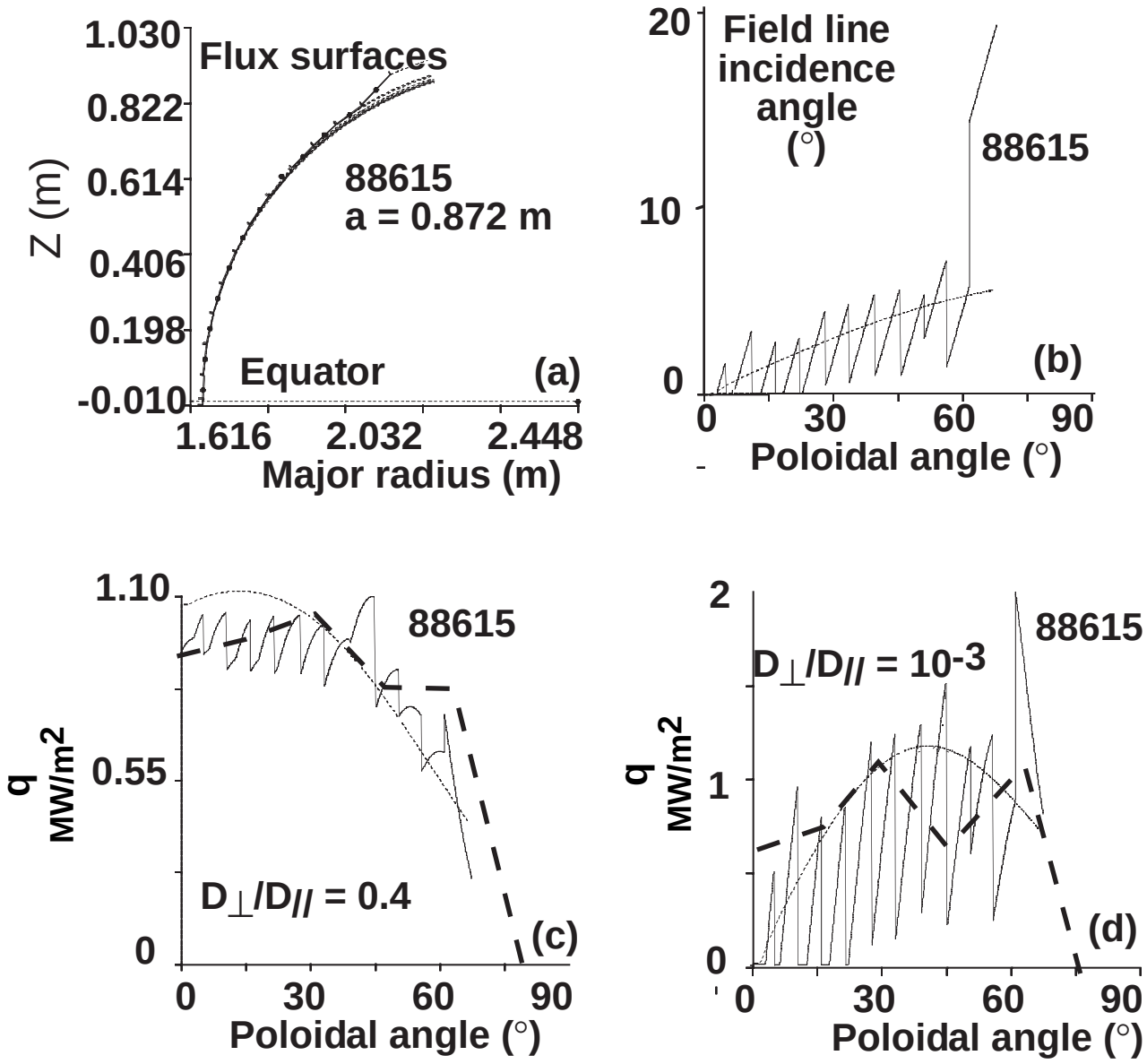

FIG. 1
Characteristics of the TFTR bumper limiter. (a) Inner bumper geometry, showing discrete tile location and flux surfaces; (b) field line angle of incidence as a function of poloidal angle for the upper half; (c, d) heat flux deposition profiles vs poloidal angle for the upper half, for cases $\Gamma\perp(0) / \Gamma\mathrm{ll}(0) = 0.4, 0.001$; the simulated D_α signal from HAIFA spectroscopy for flux distributions are shown as dashed lines

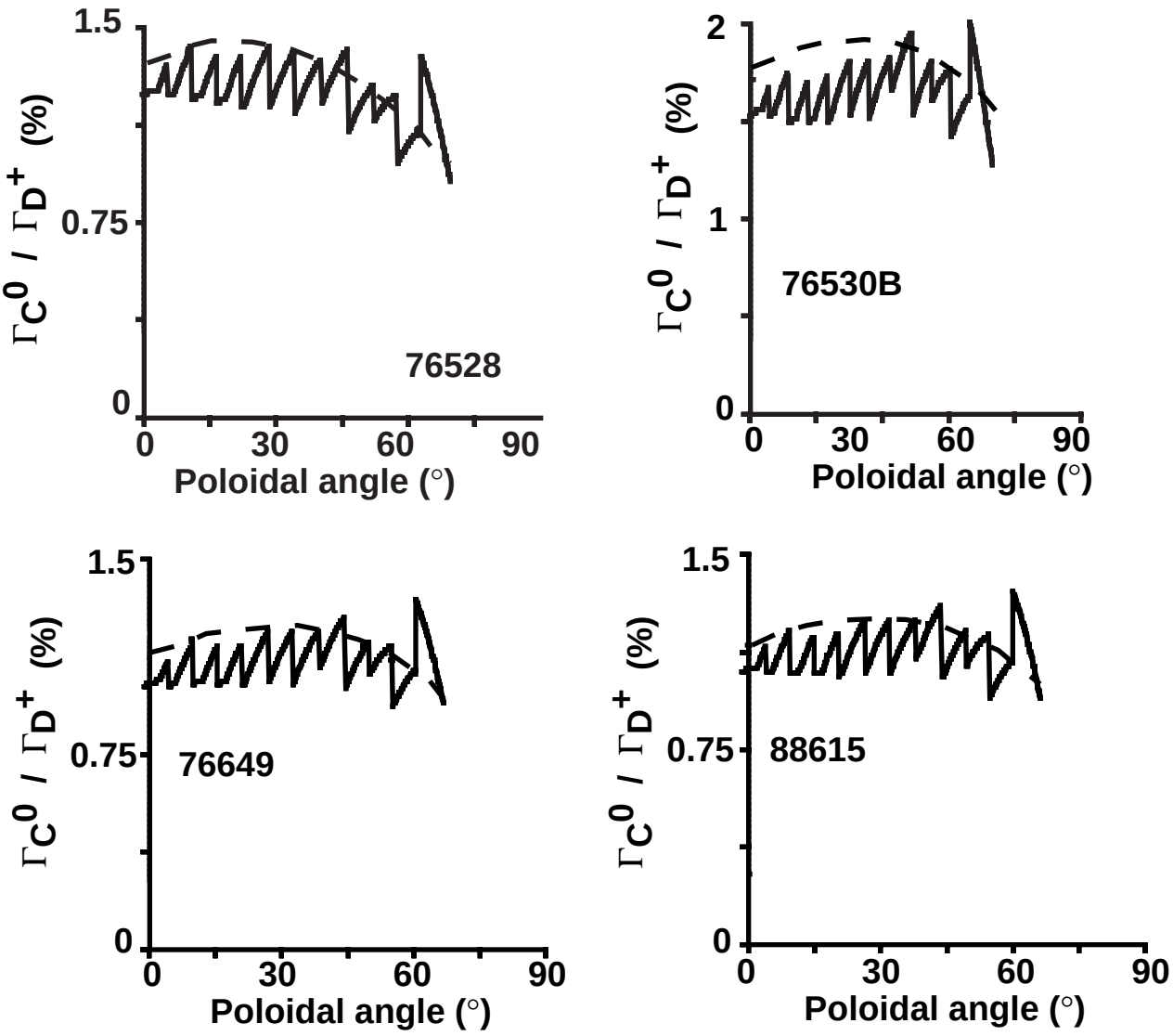

FIG. 2
Calculated local effective sputtering yield distributions
(emitted impurity flux / incident D^+ flux)
for the four cases of Table 2, with $\Gamma_\perp (0) / \Gamma_{//}(0) = 0.4$

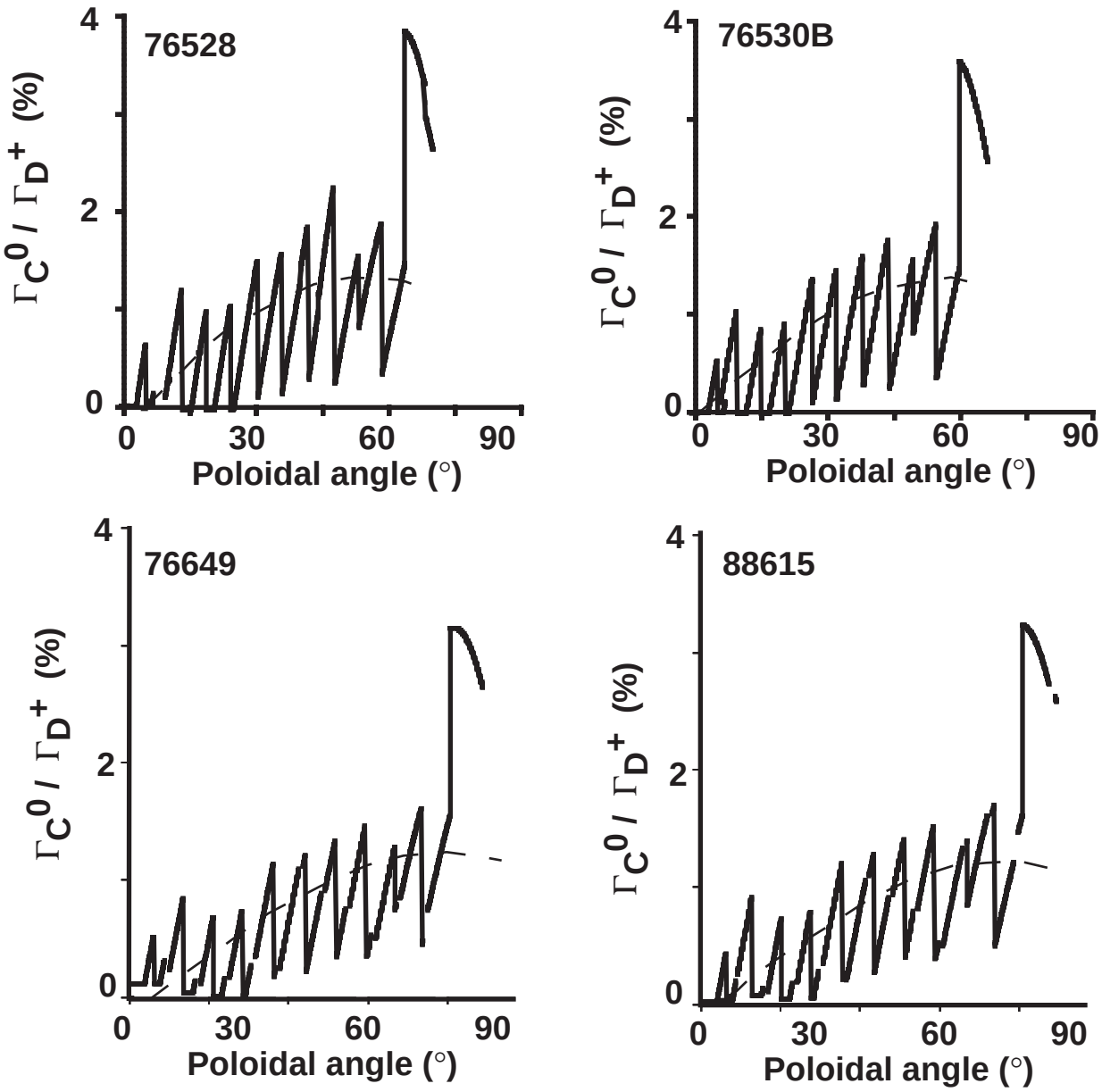

FIG. 3

Calculated local effective sputtering yield distributions (emitted impurity flux / incident D^+ flux) for the four cases of Table 2, with $\Gamma_\perp (0) / \Gamma_{//}(0) = 0.001$

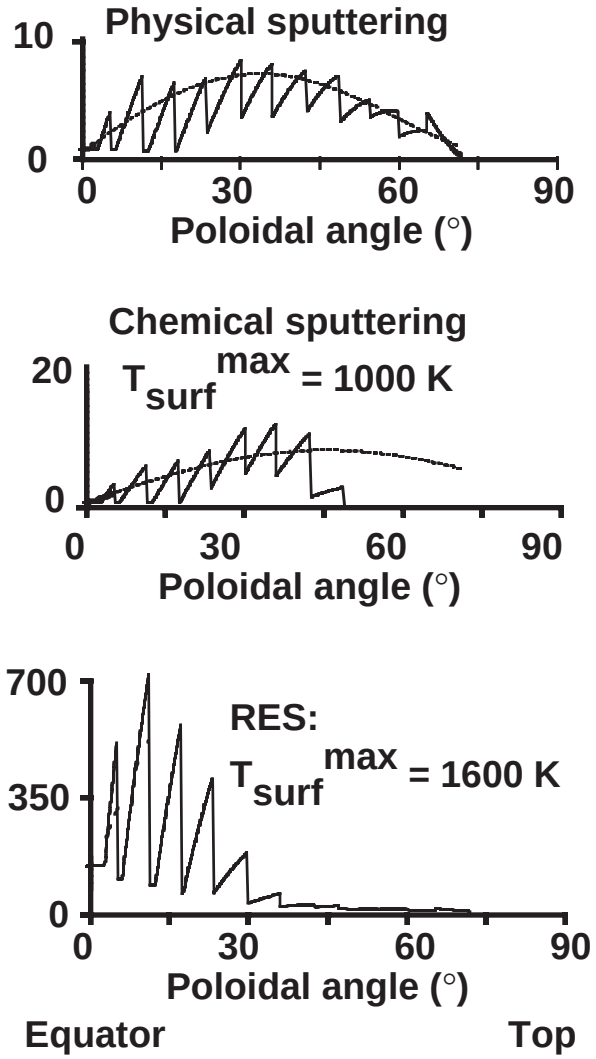

FIG. 4
Calculated local effective sputtering yield distributions (emitted impurity flux / incident D+ flux, %) for (top) physical sputtering, (middle) chemical sputtering (T_{wall}^{max} = 1000K) and (bottom) RES (T_{wall}^{max} = 1600K)